

Modelling of concentration profiles in thermally poled glasses and correlation with refractive index profiles

Petar Pervan, Jordi Sancho-Parramon, Boris Okorn, Vesna Janicki*

Vesna.Janicki@irb.hr

Ruđer Bošković Institute, Bijenička cesta 54, Zagreb 10000, Croatia

Abstract

Moderately elevated temperature and high electric field in glass poling process drift alkali ions and produce a depletion region in glass. KF9, BK7 and soda-lime glasses were poled to better understand how optical properties of glass are influenced by poling. Refractive index profiles of poled glasses were correlated to their ionic compositions, and numerical simulations generalized to arbitrary number of mobile species were performed to elucidate the dynamics of poling process. Comparison of concentration profiles derived from SIMS data and concentrations obtained from simulations verified theoretical model. It was found that refractive indices of poled glasses without Ca and Mg are higher at the surface than in depletion region. Effective ionic mobilities of Na^+ , K^+ , Mg^{2+} , Ca^{2+} , Ba^{2+} and H^+ in mentioned glasses were found from simulations. Higher refractive index near the surface was correlated with changes in glass matrix density. Modelled refractive index profiles were consistent with experiment. The research presented here brings new insights in correlation of compositional and structural changes with optical properties of glass with possible applications in optical device design and photonics.

Keywords: glass poling, thermal poling, refractive index profile, ionic mobility in glass, ellipsometry, secondary ion mass spectroscopy, numerical simulation

Introduction

During glass poling (GP) glass sample is exposed to moderately elevated temperature and high electric field. Positive alkali and earth alkali ions are drifted towards the cathode under the influence of electric field. Positive ions accumulate at some depth in glass and diffuse at the substrate-cathode interface while sub-anodic region, also referred to as depletion region (depletion zone), is depleted of these ions. The imbalance in ion distribution induces internal electric field [1, 2]. GP also known as thermal poling and until the 90s referred to as glass polarization, was first developed for use in microelectronics industry by Wallis and Pomerantz [3, 4] for glass-to-metal sealing (anodic bonding). Proctor and Sutton have demonstrated space-charge build-up during the process [5], Carlson et. al have given theoretical model of the process and provided further experimental data [6-9]. The mixed ion effect or mixed alkali effect in glasses states that if 2 alkali ions are present in a glass matrix, its electrical conductivity is reduced compared to that of glasses containing only one of these ion species [10]. There are several theories that try to explain the phenomenon, but none is universally accepted yet [11].

The hydrogen (H^+) ions from atmosphere replace alkali and earth alkali ions in sub-anodic depletion region [12]. In case there is a lack of cations, switching of non-bridging oxygen (NBO) bonds to bridging oxygen (BO) bonds [13, 14], and bonding of oxygen ions in interstitial spots takes place to form molecular oxygen. Formation of BO from NBO also leads to restructuring of the silicate network to a “silica-like” structure with higher density than the starting NBO containing matrix [15].

The process described in previous paragraph occurs in an open anode setup, but there are three possible positive electrode setups: blocking or closed anode setup in which external charge carriers cannot penetrate the anode-sample interface, non-blocking or open anode setup in which charge carriers from outside the system compensate negative charge surplus [6, 16] and semi-blocking or semi-open anode setup. Semi-blocking anode setup enables H^+/H_3O^+ diffusion into glass, but not to so high extent that would hold alkalis with mobility lower than Na^+ , such as Ca^{2+} and Mg^{2+} , to remain close to the surface, as is the case in corona non-blocking [17] or non-contact setup [18].

GP decreases refractive index (n) in sub-anodic layer of glasses containing alkali/earth alkali ions due to drift of alkalis into the glass bulk. To this point Oven published work on refractive index profile i.e. refractive index as a function of depth d - $n(d)$ of BK7 [19] and soda-lime[20] glasses while Janicki and Lipovskii groups published articles on $n(d)$ of poled soda-lime glass [21, 22]. n in depletion region of BK7 was considered constant and lower than bulk n [19] because there is no evident gradient of concentration of alkalis in depletion region. It was assumed that Si concentration is constant due to Si being a glass former [23]. In the case of soda-lime glass (SL in further text) results of modelling of $n(d)$ have shown constant n of depletion region [20]. Peak in $n(d)$ next to the bulk region of SL was reported in [21], possibly originating from accumulation of Ca and Mg. The peak was confirmed in [22] where it was stated that Ca ions accumulation is the reason for increase in n . Lou et al., however, introduced $n(d)$ model of poled SL glass with a dip in n between surface and bulk of poled glass [24].

Si concentration profile of poled glass obtained by secondary ion mass spectrometry (SIMS) shows change that supports higher Si density in sub-anodic region [23]. These results have been subject of different interpretations since the change of Si signal in SL matrix canal may be a consequence of different etching rate in different zones of poled glass [25, 26]. Measurement of concentration by glow discharge – optical emission spectroscopy technique (GD-OES) where the measurement intensity of element is directly correlated to its concentration, confirmed that change in intensity signal of Si in SIMS is mostly a consequence of changes in glass matrix [18].

In this article the origin of $n(d)$ variation of poled SL glass was investigated by correlating individual ionic species contribution to polarizability (and $n(d)$). BK7 and KF9 glasses $n(d)$ characterization was also improved upon with respect to previous work and investigated in similar manner. Furthermore, the effect of variable Si concentration in the depleted region and its effect on the $n(d)$ of poled glass is investigated.

In the scope of research in this work, optical measurements of poled glass samples were performed, and $n(d)$ obtained from the measurements. Polarizability profiles of poled samples were then obtained from $n(d)$. Poled samples were measured with SIMS, and atomic percent (at%) profiles of atomic species were obtained from the SIMS data. Numerical simulations of ionic composition in glass during GP were performed. The polarizability profiles obtained from $n(d)$ and the polarizability profiles proportional to SIMS concentrations of ionic species were correlated. At% derived from SIMS data and numerical simulation results were also compared to verify theoretical model. As a result of this comparison several findings were deduced: refractive index of layer adjacent to surface of glass is higher than at some depth in the depletion zone in glasses without Ca and Mg. Higher n is

correlated with changes of Si concentration. Modelled and theoretical $n(d)$ profiles are consistent with experiment, confirming the validity of multipole ion drift and diffusion model employed in simulations. The approach reveals the difference in three common types of silicate glasses employed in GP. These findings bring new insights on the $n(d)$ of poled glasses, and this can be important for design of optical devices and photonic applications of GP.

Theory

Theoretical background of glass poling process was explored first by von Hippel in alkali-halide crystals [27] and by several groups in silicate glasses [7, 11, 16, 28-35]. Modelling in the mentioned works was done with up to two intrinsic species.

Modelling of glass poling processes has been usually performed assuming that the process can be entirely represented by the drift and diffusion of alkali and earth alkali species, neglecting, among others, possible chemical processes (NBO to BO changes), or dependences of diffusion and mobility coefficients on the ion concentration. In this framework, the existing models [16] were generalized to include an arbitrary number of mobile species.

During GP process the movement of n_s different ionic species with initial concentration profiles C_{i0} is described by the following differential equations [36]:

$$(1) \quad \frac{\partial C_i}{\partial t} = \mu_i \frac{\partial(EC_i)}{\partial x} + D_i \frac{\partial^2 C_i}{\partial x^2}$$

$$(2) \quad \frac{\partial E}{\partial x} = \frac{e}{\varepsilon_0 \varepsilon} \sum_{i=1}^{n_s} q_i (C_i - C_{i0}), \quad i = 1, 2, \dots, n_s$$

where C_i is the concentration of ions of the i -th element, E is the electric field amplitude, x is the position in the glass, with $x=0$ being the glass surface next to the anode, and t is the time. The parameters μ_i , D_i , and q_i are the mobility, diffusion coefficient and charge of the i -th species, while e is the elementary electric charge, ε_0 the vacuum permittivity and $\varepsilon=7$ the static dielectric function of glass. The first equation states that the time evolution of ion concentration is given by the drift and diffusion currents (first and second right-hand term, respectively). The second equation is the one-dimensional Poisson equation and describes the spatial variation of the electric field upon redistribution of charges with respect to their initial concentration (C_{i0}).

These equations can be written in a more compact form in order to solve them numerically. First, the ion mobility and diffusion coefficients are related by the modified Nernst-Einstein equation [37-40]:

$$(3) \quad \mu_i = \frac{D_i e}{H k_B T}$$

where H is the Haven ratio around 0.3 first observed by Fitzgerald [41] and confirmed by others [42], k_B is the Boltzmann constant and T the temperature. In addition, one can introduce the following parameters:

- i) $d_0 = \sqrt{2\varepsilon_0 \varepsilon U / e C_0}$ with C_0 the initial total ion charge concentration ($C_0 = \sum_{i=1}^{n_s} q_i C_{i0}$) and U is the external applied potential
- ii) $E_0 = U / d_0$
- iii) $t_0 = d_0 / (\mu_1 E_0)$.

These parameters correspond to the maximum thickness of ion-depleted layer in blocking configuration (d_0), the resulting electric field if all the potential is applied in d_0 (E_0) and the time

that the carriers of the first species ($i = 1$) need to cross the region d_0 when E_0 is applied (t_0). Using these parameters, one can define dimensionless time ($\tau = t/t_0$) and position ($s = x/d_0$) coordinates and functions ($p_i = C_i/C_0$ and $f = E/E_0$). Then equation (1) and (2) can be reformulated as:

$$(4) \quad \frac{\partial p_i}{\partial \tau} = \gamma_i \frac{\partial(f p_i)}{\partial s} + \nu_i \frac{\partial^2 p_i}{\partial s^2}$$

$$(5) \quad \frac{\partial f}{\partial s} = \sum_{i=1}^{n_s} (q_i p_i) - p_0, \quad i = 1, 2, \dots, n_s$$

with $\gamma_i = \mu_i/\mu_1$, $\nu_i = \gamma_i H k_B T / (q_i e U)$ and $p_0 = \sum_{i=1}^{n_s} q_i C_{i0} / C_0$.

Solving these differential equations requires initial and boundary conditions that will depend on the specific problem (ion types, blocking/non blocking conditions). In glass poling experiments under application of a constant voltage, the following boundary condition can be imposed:

$$(6) \quad \int_0^L f ds = 1$$

where $L = W/d_0$ is the normalized sample thickness and W is its physical thickness. Numerical solution of these equations is studied for several cases using the ODE15s algorithm implemented in MATLAB.

Experimental

Preparation of the glass samples

Slabs of three different types of glass were used in the scope of research: BK7 (borosilicate) - 25 mm in diameter and 1 mm thick, KF9 (crown) - square slide with 15 mm sides, 1 mm thick, and SL (Menzel microscope glass slide) - 1 mm thick with a surface of approximately 25 mmx15 mm (cut with diamond knife from a larger slab). Both sides of all the glass substrates were cleaned by cotton wool soaked with ethanol and wiped with cotton cloth. SL glass was cleaned by cotton wool soaked with acetone and wiped with cotton cloth in order to remove the antistick coating, and afterwards cleaned in the same way as other glass types. N₂ was blown using a pressure nozzle to remove any residue from the surface of the glass substrate.

SL glass composition in weight percent (wt%) is given by the producer [43]. The composition of KF9 and BK7 glasses was determined with particle induced X-ray emission (PIXE) and time-of-flight elastic recoil detection analysis (TOF-ERDA) analysis performed at Ruđer Bošković Institute. KF9, BK7 and SL glass composition data are given in Table 1. At% is given in Table 2.

	wt% (SiO ₂)	wt% (Na ₂ O)	wt% (CaO)	wt% (MgO)	wt% (Al ₂ O ₃)	wt% (K ₂ O)	wt% (TiO ₂)	wt% (B ₂ O ₃)	wt% (BaO)
KF9	70.6±2.9	22.3±1.4	-	-	-	1.3±0.1	6.4±0.5	-	-
BK7	71.7±3.0	7.9±0.5	-	-	-	10.8±0.7	-	10.9±0.7	1.14±0.08
SL	72.2	14.3	6.4	4.3	1.2	1.2	-	-	-

Table 1: Glass composition given in molecular weight percent.

	at%(Si)	at%(O)	at%(Na)	at%(Ca)	at%(Mg)	at%(Al)	at%(K)	at%(Ti)	at%(B)	at%(Ba)
KF9	24±1	57±3	14.7±0.9	-	-	-	0.57±0.06	1.2±0.1	-	-
BK7	24±1	59±3	5.1±0.3	-	-	-	4.6±0.3	-	6.3±0.4	0.15±0.01
SL	24.7	60	9.5	2.4	2.2	0.6	0.5	-	-	-

Table 2: Glass composition given in at%.

Experimental set-up

The Cr coated BK7 glass electrode (anode) was cleaned with cotton soaked with ethanol and puffed with manual air dust blower. Both electrodes have surface area greater than the surface of the sample. Glass samples were placed between electrodes as presented in Figure 1. The whole setup is placed in the Lindberg Blue M Thermo Scientific oven. The electrodes were connected in the circuit consisting of Keithley Instruments 2290-5 voltage source, Agilent Technologies 34410A multimeter and computer. Additionally, KF9 sample was poled in Elektrosanitarij LPT60-500 oven in vacuum ($4 \cdot 10^{-4}$ hPa).

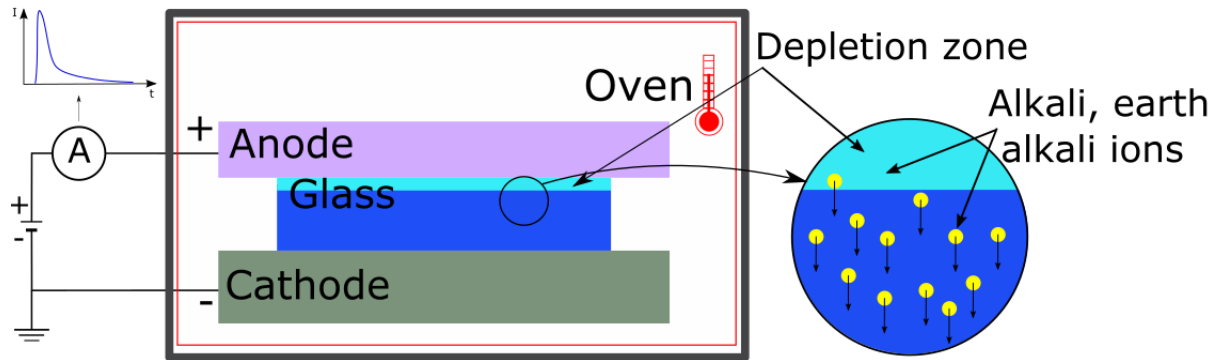


Figure 1. Schematic of GP experimental setup (left). Drift of alkali and earth alkali ions and formation of the depletion zone during the process (right).

Glass poling conditions

Conditions maintained in the experiments are as follows: 300 °C, 500 V, 2 h with the preheating period of 40 min in order to increase the thermodynamic energy of the system and to reach a stable final temperature of 300 °C before poling starts. When the preheating period was completed, the voltage was increased by 50 V increments to obtain the final voltage of 500 V. Time was measured since the final voltage was achieved. When the time of 2 h expired the voltage source and oven were turned off and the oven lid immediately opened. The sample was naturally cooled down to room temperature, and its backside was cleaned with cotton soaked with ethanol and blown with N₂ pressure nozzle prior to the measurements.

SIMS

The samples were analysed with secondary ion mass spectrometry (SIMS) using The Hiden Analytical SIMS Workstation which revealed ion intensity in dependence on duration time of SIMS of the poled sample. Primary ions used were O²⁺. The final depth of the etched crater was measured with Bruker Dektak XT™ stylus profilometer. Data obtained from SIMS was used to calculate at% profile of poled samples. Intensity of particular ionic species in poled glass obtained by SIMS was multiplied by its known at% of the same ionic species of virgin glass and the resulting value divided by the averaged bulk glass SIMS intensity of the same ionic species. This should allow correlating individual atomic species contribution to polarizability and *n*. Vacuum poled sample was not analysed by SIMS.

Ellipsometry

Ellipsometric measurements were performed on J. A. Woolam VASE ellipsometer in the 0.57-3.8 eV range at 45°, 55° and 65° incidence angles. Ellipsometry was used to measure ellipsometric Ψ and Δ functions, from which optical constants, poling depths and $n(d)$ were obtained.

Optical characterization of the samples was performed using J. A. Woolam WVASE software package. The optical constants were fitted to experimental data with Sellmeier oscillator in every layer.

Sellmeier model employs Lorentz oscillators with zero broadening, so they only affect the real part of the dielectric function. This allows the light-matter phenomena outside of the measured range that influence dielectric function (and refractive index) in the measured range, to be taken into account. In the course of optical characterization the sample is modelled as a multilayer system where refractive index parameters and thickness of each layer is optimized to give the best fit of the models optical properties to the measured data. The layers are modelled with either constant refractive index (homogeneous layer) or with refractive index changing as an exponential function of the thickness (inhomogeneous layer). However, the latter case is defined as a number of thinner homogeneous sublayers in the characterization software. In the course of optical characterization it is important to keep the number of models layers reasonably low to avoid too much optimization parameters that could lead to the unreliable or unrealistic solutions. For this reason no effort was made here to obtain smooth or more detailed refractive index profile. The model is limited to a rather rough and simple multilayer system giving step-wise refractive index profile but having optical properties that fit well the measured data. It should be noted that the modelling of ellipsometric data for each sample starts from the simplest, one layer model and the new parameters are introduced gradually. If the new parameter significantly decreases discrepancy between experimental data and the fit, it is kept.

Numerical simulations

Numerical simulations were written and performed in Mathworks MATLAB software.

The Lorentz-Lorenz model was used in numerical simulations for comparing polarizability calculated from SIMS and ellipsometry. Lorentz-Lorenz equation is given as:

$$(7) \quad \frac{n^2-1}{n^2+2} = \sum_i \frac{N_i \alpha_i}{3\epsilon_0},$$

as a sum over all the species i that contribute to material polarizability, where N_i is the number of molecules per unit volume and α_i is the molecular polarizability. In order to take into account contribution of silica matrix densification suggested by SIMS data, Si concentration is taken constant only in bulk region, while in depletion region is defined as linear function.

The ionic mobilities of SL glass obtained in experiments [12] and used in simulations by Petrov et al. [16] are $\mu(\text{Na}) = 7 \cdot 10^{-16} \text{ m}^2(\text{Vs})^{-1}$, $\mu(\text{H}) = 2 \cdot 10^{-20} \text{ m}^2(\text{Vs})^{-1}$ and $\mu(\text{Ca}) = 1 \cdot 10^{-21} \text{ m}^2(\text{Vs})^{-1}$ at 150 °C. Duration of experiment and simulation was 540 s, and voltage applied was 1.7 kV. Brennan et al. experimentally found ionic mobility of sodium in SL glass at 200 °C: $\mu(\text{Na}) = 5.3 \cdot 10^{-15} \text{ m}^2(\text{Vs})^{-1}$, and of BK7 $\mu(\text{Na}) = 5.4 \cdot 10^{-15} \text{ m}^2(\text{Vs})^{-1}$ and crown glass $\mu(\text{Na}) = 8 \cdot 10^{-15} \text{ m}^2(\text{Vs})^{-1}$ at 300 °C [44]. All samples were poled for 90 minutes, while voltage was increased linearly with time to maintain constant current of 20 μA . Oven used $\mu(\text{Na}) = 1.3 \cdot 10^{-15} \text{ m}^2(\text{Vs})^{-1}$, $\mu(\text{H}) = 1.3 \cdot 10^{-19} \text{ m}^2(\text{Vs})^{-1}$ and $\mu(\text{K}) = 1.625 \cdot 10^{-17} \text{ m}^2(\text{Vs})^{-1}$ at 300 °C in numerical and analytical simulations of poling of SL and borosilicate glasses. This analysis was based on the solution of the drift-diffusion equation on the assumption of a constant ion injection rate, j , rather than a defined voltage boundary condition [34]. These values were used as an initial guess in our simulations, and were eventually modified to fit atomic concentration profiles obtained from SIMS measurements.

The simulations performed by Petrov et al. and Oven involved two intrinsic ionic species. In the scope of research performed in this article two ionic species are considered in KF9, three in BK7 and four in SL. The temperature, voltage and time duration are the same as in experiments, $T=300$ °C, $V=500$ V and $t=2$ h. Sample thickness is 1 mm and static dielectric constant of glass is fixed at $\epsilon=7$.

The presumption of the model is that H^+ ions are abundant to penetrate the air/glass interface during the whole process.

Results

Figure 2 shows Ψ (a, c and e) and Δ (b, d and f) ellipsometric functions experimental data and fits for virgin and poled glasses. There is visible change (fringes) in Ψ of poled samples in comparison to Ψ of the virgin glass, which leads to conclusion that GP changed n of the glass

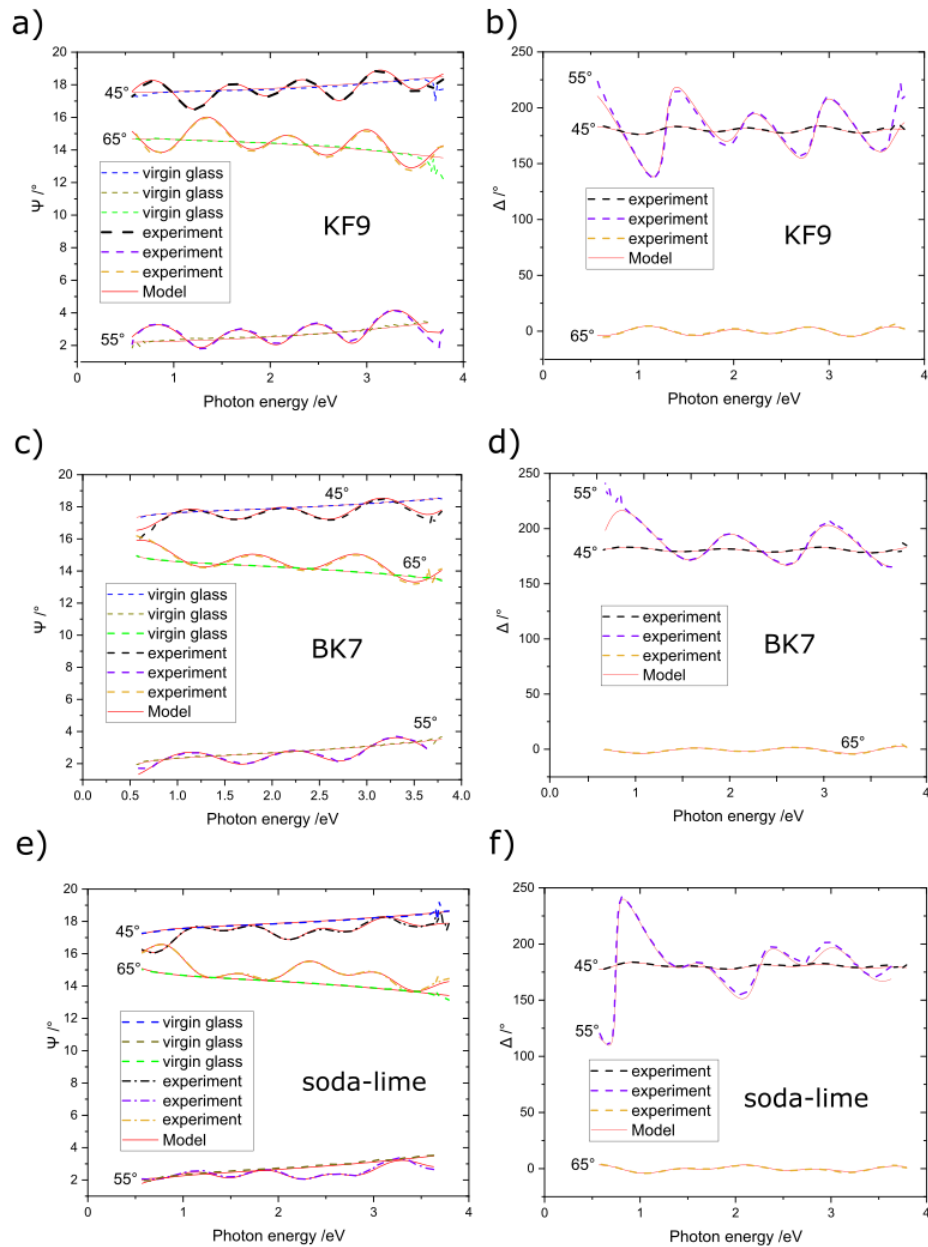


Figure 2. Measured and fitted ellipsometric Ψ (left) and Δ (right) functions of virgin and poled KF9, BK7 and SL glasses at three incidence angles.

Figure 3 presents $n(d)$ of KF9, BK7 and SL samples poled in air, and KF9 sample poled in vacuum. SL glass $n(d)$ presents n peak in front of bulk region, that is in accordance with [21] where is suggested it may be a consequence of Ca and Mg ion accumulation in this region. KF9 and BK7 glass are free

from Ca and Mg, so no pile up of alkali earth ions concentration and peak in n should be expected and $n(d)$ should be constant. However, it decreases until minimum at the depth of approximately 300-500 nm. Poling of KF9 was made in vacuum as well and the resulting profile shows the same trend as in the case of poling in air. In the case of BK7, n increases a bit before it reaches the bulk value.

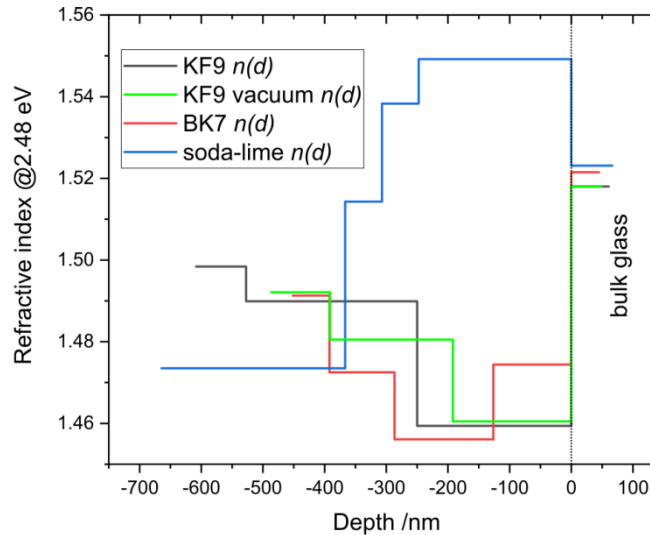


Figure 3. $n(d)$ of KF9 poled in air and vacuum, BK7 and SL glass poled in air. *Interface between zones is at 0 nm: positive values present bulk and negative depletion zone.*

Figure 4. presents intensities of Si, alkali and earth alkali ions in KF9, BK7 and SL glasses obtained by SIMS compared with $n(d)$ obtained by ellipsometry. It should be noted that in all the cases Si signal decreases in near-surface volume of samples, which is depleted of alkali and earth alkali ions. In the case of KF9 glass, the decrease of Si signal is approx. 35% in approx. 520 nm of the depleted region. Comparing with KF9 $n(d)$, this corresponds well with the decrease of n (from 1.498 at the surface to 1.459, $\Delta n=0.039$ in 608 nm). Thickness discrepancy between SIMS and ellipsometry based model here is 15%. For BK7 glass, the decrease of Si signal is approx. 30% in 300 nm before Ba accumulation (Figure 4 (b)). Comparing with BK7 $n(d)$, this again corresponds well with n decrease (from 1.491 at the surface to 1.456, $\Delta n=0.039$ in 326 nm). Thickness discrepancy between SIMS and ellipsometry based model for this sample is 12%.

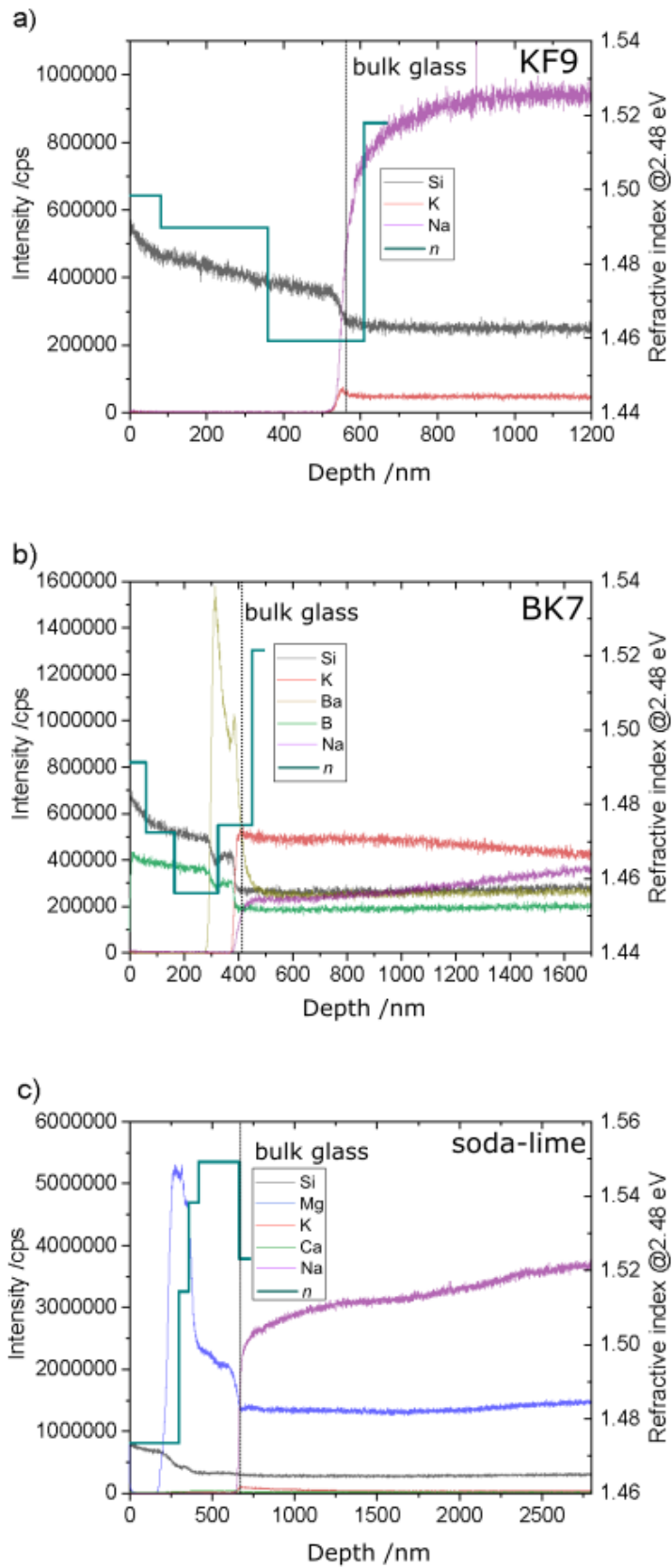


Figure 4. a) KF9, b) BK7 and c) SL SIMS intensity vs. $n(d)$. Air/glass interface is at 0 nm, and bulk is at positive values.

Figure 5. presents the polarizability profiles of KF9, BK7 and SL obtained as a sum of individual contributions of ionic species, assumed to be proportional to the SIMS concentration, [fitted to \$n\(d\)\$ profiles obtained from ellipsometric measurements](#). The following equation was used:

$$(8) \quad \frac{n^2-1}{n^2+2} = \sum_{i=1}^N A_i I_i,$$

where A_i is a proportionality constant and I_i is calculated from SIMS concentration for i -th species contributing to polarizability. Figures 5 (b), (d) and (f) show the individual contributions from Na^+ , K^+ , Ca^{2+} , Mg^{2+} and Ba^{2+} . A_i was obtained by fitting the polarizability profiles found from SIMS concentrations to the polarizability found by ellipsometry according to the Equation 8. Only, instead of Si SIMS data, a linear variation of Si concentration due to possible matrix densification was used. A re-scaling parameter was optimized to account for possible differences in depth of SIMS and ellipsometry. The depletion zone depths used for atomic contribution simulations are 550, 390 and 380 nm for KF9, BK7 and SL glass, respectively. Thickness discrepancy between SIMS and ellipsometry based model for SL sample is 3%.

In the case of KF9, polarizability has the lowest value at the edge of the depletion zone, while in bulk and near-surface it has higher values. In the case of BK7 increase in polarizability in front of bulk region coincides well with accumulation of Ba from SIMS measurements. Results for SL sample show polarizability peak in front of bulk region corresponding to accumulated Ca^{2+} ions presenting high contribution to polarizability. Na^+ contribution is significant, while K^+ and Mg^{2+} polarizability influence [seems to be nearly negligible](#). [One has to keep in mind that the influence of each individual specie to the total polarizability depend on at% of the specie in glass](#). For example, Na^+ influence on polarizability is the highest in KF9, lower in SL and the lowest in BK7 and K^+ influence is very low in KF9 and SL (less than 1 at% of K^+), while in BK7 (4.3% of K^+) it is considerable. This is in agreement with at% (Table 2) and graphs of at% calculated from SIMS data (Figure 6 (a), (b) and (c)).

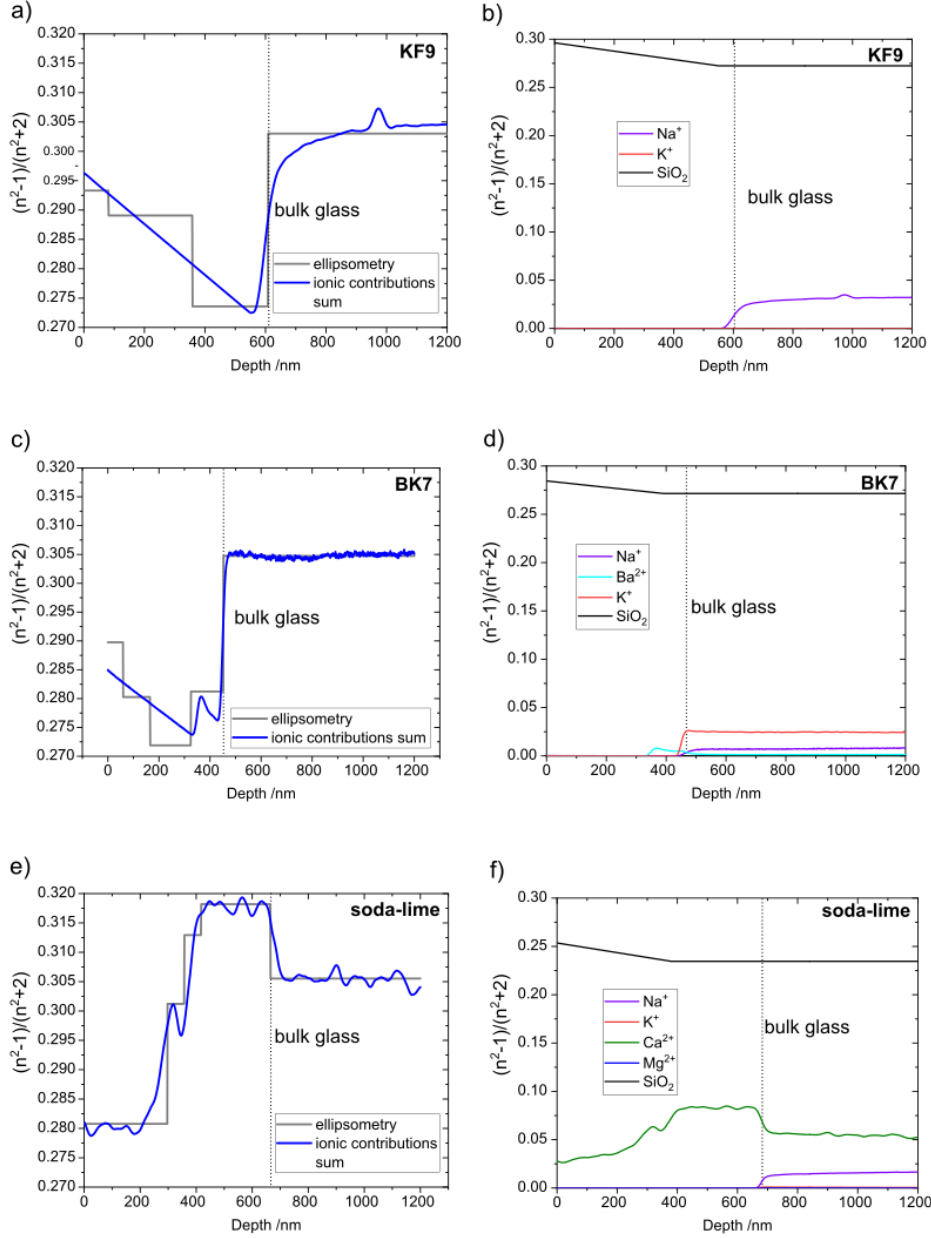


Figure 5. a), c) and e) Polarizability profiles, defined in Equation 8., of KF9, BK7 and SL glasses, respectively, obtained from optical characterization and SIMS measurement, b), d) and f) polarizability contribution from individual atomic species contained in KF9, BK7 and SL, respectively, obtained from simulations. Air/glass interface is at 0 nm, and bulk is at positive values.

Comparison of at% profiles of the poled samples calculated from experimental SIMS data and from numerical simulations of the KF9, BK7 and SL samples are given in Figure 6. The figure shows good agreement of experimental and simulated at% for these types of glasses. High concentration of H^+ ions in simulation is a consequence of assumed abundance of H^+ at the air/glass interface. The final mobilities obtained in simulations are given in Table 3.

	$\mu(\text{Na})/\text{m}^2(\text{Vs})^{-1}$	$\mu(\text{Ca})/\text{m}^2(\text{Vs})^{-1}$	$\mu(\text{H})/\text{m}^2(\text{Vs})^{-1}$	$\mu(\text{K})/\text{m}^2(\text{Vs})^{-1}$	$\mu(\text{Mg})/\text{m}^2(\text{Vs})^{-1}$	$\mu(\text{Ba})/\text{m}^2(\text{Vs})^{-1}$
Menzel	$5.4 \cdot 10^{-15}$	$= 9 \cdot 10^{-20}$	$2 \cdot 10^{-20}$	$2 \cdot 10^{-15}$	$3 \cdot 10^{-20}$	-
BK7	$5.4 \cdot 10^{-15}$	-	$2 \cdot 10^{-20}$	$2 \cdot 10^{-15}$	-	$1.6 \cdot 10^{-20}$
KF9	$5.4 \cdot 10^{-15}$	-	$4.2 \cdot 10^{-20}$	$2 \cdot 10^{-15}$	-	-

Table 3. Ionic mobilities of Menzel, BK7 and KF9 glasses

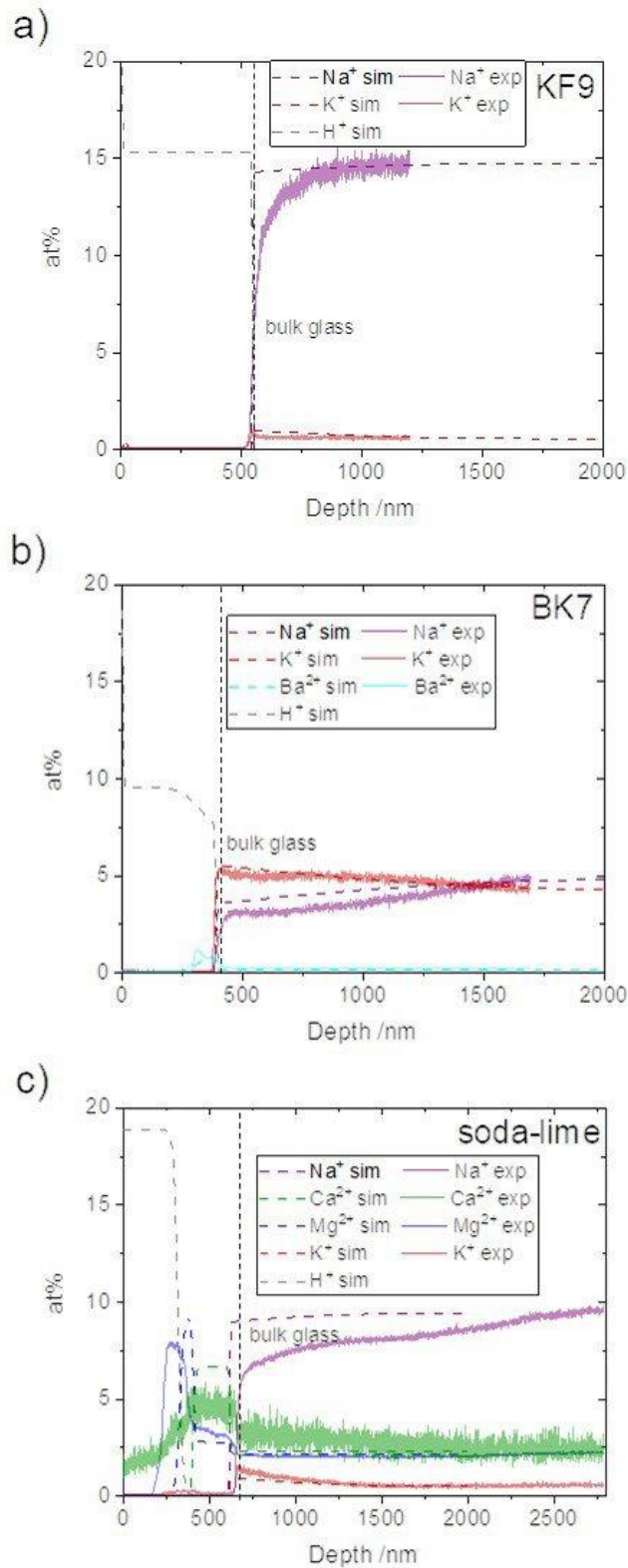


Figure 6. Comparison of at% profiles of a) KF9, b) BK7 and c) SL glass obtained from simulations and SIMS measurements. Air/glass interface is at 0 nm, and bulk is at positive values.

Discussion

The optical properties of final models obtained from optical characterization are in very good accordance with the measured data. The models are not complex as they contain low number of

parameters (3-4 layers, each layer 3-5 parameters). Therefore, the obtained $n(d)$ may be taken as reliable results.

While $n(d)$ profile for SL is consistent with [21], the profiles for KF9 and BK7 present minimum value in front of bulk region. The result is consistent also for KF9 poled in vacuum. The question is: what is the origin of the n decrease towards bulk in KF9 and BK7 glasses. SIMS data do not suggest mobile species concentration profile that could give explanation to the obtained $n(d)$. At the other hand, one can notice nearly linear decrease of Si signal towards bulk region for both samples (Fig.4.). Comparing SIMS data and $n(d)$ it is possible to conclude that the origin of the $n(d)$ decrease and appearance of refractive index minimum in depleted region is the change in silica matrix density.

As mentioned previously, GP in this work was done with pressed electrodes, that present semi-open (semi-blocking) poling setup [45]. This means that the supply of H^+/H_3O^+ ions is not sufficient to compensate the lack of positive charge, so it is expected that NBO transforms to BO by the release of O^- and formation of Si-O-Si bonds. This is accompanied by the increased number of members in SiO_4 tetrahedra rings, altogether increasing the matrix density towards the silica-like one [13, 18, 50]. Transformation rate of NBO to BO and/or increase of tetrahedra ring members is not uniform throughout depleted layer but is higher closer to the anode due to the lack of positive species to compensate alkali drift. Increased matrix density leads to the increase in n (and polarizability) that is in accordance with presented profiles. Similar fingerprint of silica matrix restructuring, although indicated by Si SIMS data, was overlooked and not included in previous study of poled SL glass $n(d)$ [21]. The reason for this was presence of Ca^{2+} pile up next to the bulk region, which meant modelling demanded significant number of parameters. Also, Ca^{2+} pile up influence on $n(d)$ partially masks the contribution of matrix restructuring in a relatively thin sub-anodic layer of 200 nm or less. Therefore, glasses without earth alkalis represent simpler systems where it is easier to distinguish matrix densification contribution to $n(d)$.

It is possible to roughly estimate expected values of n due to silica matrix restructuring and compare them with the obtained results. The most compact type of SiO_2 matrix is its crystalline form, i.e. quartz, with $n=1.55$ at 500 nm (2.48 eV) (Table 4). The amount of impurities, NBO and SiO_4 tetrahedra rings with less than four members should be negligible. Its glassy form (significant concentration of less than four member SiO_4 tetrahedra rings), fused silica, has less dense structure with n equal to 1.462-1.466 at 500 nm (2.48 eV) (depending of grade, content of Si-OH bonds may be from couple of tens to couple of hundreds ppm, not influencing n in visible range significantly) [46]. Densities and n of KF9 and BK7 are between values for quartz and fused silica. Besides silica, as the main matrix former, these glasses contain 10.9 wt% B_2O_3 (BK7) and 6.4 wt% TiO_2 (KF9) and significant amount of NBO bonds neutralized by alkali and earth alkalis. Minimal n obtained upon GP is around 1.46 that is somewhat lower than the value for fused silica. The obtained minimal value corresponds to the structure depleted of alkalis and not filled with other species, with matrix density lower than fused silica one. At the same time, maximal n is significantly higher in the near-surface depth, around 1.49-1.5, but still lower than virgin glass or quartz. The structure in this region is also alkali depleted, but density (and n) is more silica-like due to matrix restructuring by NBO transforming to BO and SiO_4 tetrahedra rings gaining more members in sub-anodic region. Using effective medium approximation, simulation of the mixture of fused silica with 3.6 vol% of TiO_2 (corresponding to 6.4 wt% TiO_2 in KF9) results in effective n value 1.485 (at 500 nm), that is in good accordance with the obtained n_{max} of KF9 sample. This mixture should roughly correspond to alkali depleted KF9 glass with fused silica matrix structure. It can be concluded that the obtained refractive index values are realistic according to the expected glass structure and composition.

	density (g/cm ³)	n (at 500 nm or 2.48 eV)	
		n _{min}	n _{max}
air poled KF9	-	1.4594	1.4984
vacuum poled KF9	-	1.4605	1.4921
air poled BK7	-	1.4561	1.4913
quartz	2.649 [47]	1.55	
fused silica	2.20 [46]	1.462-1.466 [46]	
KF9	2.50 [48]	1.5177	
BK7	2.51 [49]	1.5215	

Table 4. Density and refractive index of quartz, fused silica KF9 and BK7 glasses.

KF9 contains only highly mobile Na⁺ and K⁺, while BK7 in addition contains low amount of Ba²⁺. Although Ba²⁺ concentration is low, its ion diameter is large and therefore it can be expected it has large dipole moment and may significantly influence polarizability, [resulting in the increase of poled KF9 n in front of bulk, where it accumulated \(Figure 4. b\)](#). Polarizability contribution of Na⁺ is probably masked by the Ca²⁺ to some degree, since simulated polarizability peak (Figure 5 (f)) is fitted only with Ca²⁺. Polarizability of Ca²⁺ in bulk region is determined by the polarizability of Ca²⁺ in the peak region. The difference in at% at peak and in bulk for Ca²⁺ is approximately 2:1, so this also sets the bulk value of Ca²⁺. Polarizability of Ca²⁺ in bulk is therefore probably overestimated and the one of Na⁺ underestimated by the fit. The obtained low Mg²⁺ polarizability may be ascribed to its small radius, compared to Ca²⁺, [but also to the concentration peak overlapping with the one of Ca²⁺ and possible underestimation of its contribution by overestimation of Ca contribution in the course of numerical optimization](#). The linear model of glass matrix (Si) contribution to polarizability provided results consistent with ellipsometric models of $n(d)$.

Numerical simulations of ionic mobilities used Haven ratio equal to H = 0.3, a value within range of experimental results by Fitzgerald and others. As can be seen in Figure 6, SIMS obtained at% profiles show greater diffusion than simulation profiles. However, using higher H value in simulations deteriorates the at% profiles obtained from SIMS in comparison with at% obtained from simulations. It was previously stated that a simplified model was used, which could explain almost step-like profile of simulated at%.

Initial $\mu(\text{Na})$, $\mu(\text{Ca})$, $\mu(\text{H})$ and $\mu(\text{K})$ used in numerical simulations were taken from [16, 34, 44]. Different authors provide different values of μ , depending on the type of glass and poling conditions, but here ionic mobilities are consistent for all types of glass. $\mu(\text{K})$ was altered to get a good fit to SIMS data, while $\mu(\text{Na})$, $\mu(\text{Ca})$ and $\mu(\text{H})$ remained the same, or only slightly modified. Since the models of BK7 and SL glass were more complex than in previous works, $\mu(\text{Mg})$ and $\mu(\text{Ba})$ were found through iterating simulations and fitting the obtained profiles to SIMS experimental data.

Mobility of hydrogen ions, $\mu(\text{H})$, in KF9 is higher than in SL and BK7 glasses. The reason for this could be explained by the mixed ion effect, as follows. Since Na⁺ and K⁺ have mobilities considerably higher than other ions, and of the same order of magnitude, these two ionic species drift into the glass and leave vacancies in which other ions can jump. In KF9 there is no additional ionic species to reduce

drift of H^+ into glass matrix, while in both SL and BK7 there are: Ca^{2+} and Mg^{2+} in SL, and Ba^{2+} in BK7. This is why KF9 will allow higher effective mobility of hydrogen ions than SL and BK7.

It should be noted that non-blocking anode configuration was assumed in the numerical simulations, while the experiments were performed in a semi-blocking anode configuration. Yet, the model is able to provide a good correspondence with the experimentally determined concentration profiles. The fact that NBO to BO re-arrangement and some other effects, such as drift of negative oxygen ions toward the anode, is neglected in the model can be partially compensated by unlimited H^+ ions abundance at the air/surface interface considered in the simulations.

Conclusion

In this study we investigated GP in glasses with different composition combining several techniques that enabled obtaining novel insights in this process. Depletion zone depths and at% differ in all the samples which results in different $n(d)$. Thus, it is confirmed that polarizability (and $n(d)$) of different glasses containing alkali and earth alkali ions after poling at the same conditions is influenced by their composition.

Restructuring of silica matrix in the course of GP results in changes of polarizability and refractive index, which can be resolved from analysis of optical measurements, i.e. spectroscopic ellipsometry data. The obtained polarizability profiles of Ca^{2+} and Mg^{2+} free glasses (KF9 and BK7) depleted region are in accordance with SIMS data obtained for Si. These findings support that for the studied samples silica matrix restructuring is not uniform throughout the whole depleted region, but the changes are more pronounced in the region close to the anode surface. In the case of soda-lime glass, Ca^{2+} accumulation masks the contribution of silica matrix densification to the increase of polarizability.

The polarizability profile of KF9, BK7 and SL (Menzel) is consistent with SIMS data. High polarizability near surface of KF9 and BK7 can be attributed to denser glass matrix due to structural changes of glass matrix from NBO to BO bonds close to surface of glass. The $n(d)$ and polarizability obtained from ellipsometry corresponds well to modelled contribution of individual atomic species to polarizability obtained by numerical simulations. Ca^{2+} , Na^+ and Ba^{2+} contribute to the n the most, while K^+ and Mg^{2+} have lower influence.

At% in numerical simulations were fitted to at% calculated from SIMS. The model provided good agreement of simulated and experimental data. Numerical simulations resulted in numerical values of previously unknown parameters, such as effective ionic mobilities $\mu(Mg)$ and $\mu(Ba)$ as well as $\mu(H)$ of KF9 glass. In addition, $\mu(K)$ value is two orders of magnitude higher than the one obtained in previous work [34, 35]. The mobilities should be considered as effective mobilities due to the complex interplay of ionic species mobilities in the glass matrix with more than one intrinsic ionic species known as mixed ion effect. Haven ratios (and diffusivities) of ions in studied glasses at applied poling conditions were found to be in the range of experimentally confirmed interval.

The research presented here brings new insights in correlation of compositional and structural changes with optical properties. Better understanding of GP process will help to extend the application of this technique for optical device design and photonics.

Credit authorship contribution statement

Petar Pervan: Writing – original draft, Writing – review & editing, Visualization, Methodology, Investigation, Conceptualization, Experiment, Formal analysis, Data curation, Conceptualization.
Jordi Sancho-Parramon: Writing – review & editing, Methodology, Investigation, Conceptualization,

Software, Data curation, Formal analysis. **Boris Okorn:** Writing – review & editing, Visualization, Methodology, Investigation, Data curation **Vesna Janicki:** Writing – review & editing, Visualization, Validation, Supervision, Resources, Project administration, Methodology, Investigation, Funding acquisition, Formal analysis, Data curation, Conceptualization.

Acknowledgments

This work was financed by the Croatian Science Foundation under the projects no. DOK-2018-01-3956 and IP-2016-06-2168.

References:

- [1] P. G. Kazansky and P. St. J. Russell, »Thermally poled glass: frozen-in electric field or oriented dipoles?,« *Optics Communications*, vol. 110, no. 5-6, pp. 611-614, 1994.
- [2] T. G. Alley, S. Brueck and R. A. Myers, »Space charge dynamics in thermally poled fused silica,« *Journal of Non-Crystalline Solids*, vol. 242, no. 2-3, pp. 165-176, 1998.
- [3] D. I. Pomerantz, »Anodic bonding«. Patent US3397278 A, 1968.
- [4] G. Wallis and D. I. Pomerantz, "Field Assisted Glass-Metal Sealing," *Journal of applied physics*, vol. 40, no. 10, pp. 3946-3949, 1969.
- [5] T. M. Proctor and P. M. Sutton, »Space-Charge Development in Glass,« *Journal of the American Ceramic Society*, vol. 43, no. 4, pp. 173-179, 1 April 1960.
- [6] D. E. Carlson, K. W. Hang and G. F. Stockdale, »Electrode "Polarization" in Alkali-Containing Glasses,« *Journal of the American Ceramic Society*, vol. 55, br. 7, pp. 337-341, 1972.
- [7] D. E. Carlson, »Ion Depletion of Glass at a Blocking Anode: I, Theory and Experimental Results for Alkali Silicate Glasses,« *Journal of the American Ceramic Society*, vol. 57, no. 7, pp. 291-294, 1974.
- [8] D. E. Carlson, K. W. Hang and G. F. Stockdale, »Ion Depletion of Glass at a Blocking Anode: II, Properties of Ion-Depleted Glasses,« *Journal of the American Ceramic Society*, vol. 57, br. 7, pp. 295-300, 1974.
- [9] D. E. Carlson, »Anodic Proton Injection in Glasses,« *Journal of the American Ceramic Society*, vol. 57, no. 11, pp. 461-466, 1974.
- [10] R. H. Doremus, »Mixed-Alkali Effect and Interdiffusion of Na and K Ions in Glass,« *Journal of the American Ceramic Society*, vol. 57, no. 11, pp. 478-480, November 1974.
- [11] X. Prieto-Blanco and C. Montero-Orille, »Theoretical Modelling of Ion Exchange Processes in Glass: Advances and Challenges,« *Applied Sciences*, vol. 11, no. 11, p. 5070, 2021.
- [12] C. M. Lepienski, J. A. Giacometti, G. F. Leal Ferreira, F. L. Freire Jr. and C. A. Achete, »Electric field distribution and near-surface modifications in soda-lime glass submitted to a dc potential,« vol. 159, no. 3, pp. 204-212, 1993.
- [13] M. Dussauze, V. Rodriguez, A. Lipovskii, M. Petrov, C. Smith, K. Richardson, T. Cardinal, E. Fargin

- and E. I. Kamitsos, »How Does Thermal Poling Affect the Structure of Soda-Lime Glass?,« *Journal of Physical Chemistry C*, vol. 114, no. 29, pp. 12754–12759, 2010.
- [14] A. V. Redkov, V. G. Melehin, V. V. Statcenko and A. A. Lipovskii, »Nanoprofiling of alkali-silicate glasses by thermal poling,« *Journal of Non-Crystalline Solids*, vol. 409, pp. 166-169, 2015.
- [15] J. Luo, S. Bae, M. Yuan, E. Schneider, M. T. Lanagan, C. G. Pantano and S. H. Kim, »Chemical structure and mechanical properties of soda lime silica glass surfaces treated by thermal poling in inert and reactive ambient gases,« *Journal of the American Ceramic Society*, vol. 101, no. 7, pp. 2951-2964, 2018.
- [16] M. I. Petrov, Y. A. Lepen'kin and A. A. Lipovskii, »Polarization of glass containing fast and slow ions,« *Journal of Applied Physics*, vol. 112, no. 4, p. 043101, 2012.
- [17] A. Dergachev, V. Kaasik, A. Lipovskii, V. Melehin, A. Redkov, I. Reshetov and D. Tagantsev, »Control of soda-lime glass surface crystallization with thermal poling,« *Journal of Non-Crystalline Solids*, vol. 533, p. 119899, 2020.
- [18] M. Chazot, M. Parailous, S. Jouannigot, L. Teulé-Gay, J.-P. Salvétat, F. Adamietz, R. Alvarado-Meza, L. Karam, A. Poulon, T. Cardinal, E. Fargin and M. Dussauze, »Enhancement of mechanical properties and chemical durability of Soda-lime silicate glasses treated by DC gas discharges,« *Journal of the American Ceramic Society*, vol. 104, no. 1, pp. 157-166, 2020.
- [19] R. Oven, »Measurement of planar refractive index profiles with rapid variations in glass using interferometry and total variation regularized differentiation,« *Journal of Modern Optics*, vol. 62, p. S53–S60, 2015.
- [20] R. Oven, »Measurement of the refractive index of electrically poled soda-lime glass layers using leaky modes,« *Applied Optics*, vol. 55, no. 32, pp. 9123-9130.
- [21] I. Fabijanić, P. Pervan, B. Okorn, J. Sancho-Parramon and V. Janicki, »Ellipsometry-based study of glass refractive index depth profiles obtained by applying different poling conditions,« *Applied Optics*, vol. 59, no. 5, pp. A69-A74, 2020.
- [22] E. Babich, R. Dmitrii, E. Lubyankina and A. Lipovskii, »Depth of glass poling - via optical transmission spectra,« *Optik*, vol. 244, p. 167600, 2021.
- [23] V. P. Kaasik, A. Lipovskii, D. Raskhodchikov, I. Reshetov and D. Tagantsev, »How to reveal the correct elemental concentration profiles in poled multicomponent silicate glasses from the data of secondary ion mass spectrometry (SIMS),« *Journal of Non-Crystalline Solids*, vol. 503-504, pp. 397-399, 2019.
- [24] J. Luo, H. He, N. J. Podraza, L. Qian, C. G. Pantano and S. H. Kim, »Thermal Poling of Soda-Lime Silica Glass with Nonblocking Electrodes—Part 1: Effects of Sodium Ion Migration and Water Ingress on Glass Surface Structure,« *Journal of the American Ceramic Society*, vol. 99, no. 4, pp. 1221-1230, 2016.
- [25] N. J. Smith, C. T. McLaren and A. J. Fahey, »Comments on “How to reveal the correct elemental concentration profiles in poled multicomponent silicate glasses from the data of secondary ion mass spectrometry (SIMS)”,« *Journal of Non-Crystalline Solids*, vol. 522, p. 119547, 2019.

- [26] V. P. Kaasik, A. A. Lipovskii, D. V. Raskhodchikov, I. V. Reshetov and D. K. Tagantsev, »Response to comments on "How to reveal the correct elemental concentration profiles in poled multicomponent silicate glasses from the data of secondary ion mass spectrometry (SIMS)",« *Journal of Non-Crystalline Solids*, vol. 523, p. 119553, 2019.
- [27] A. von Hippel, E. P. Gross, J. G. Jelatis and M. Geller, »Photocurrent, Space-Charge Buildup, and Field Emission in Alkali Halide Crystals,« *Physical Reviews Journal*, vol. 91, no. 3, p. 568, 1 August 1953.
- [28] M. Abou-El-Leil and A. R. Cooper, »Analysis of Field-Assisted Binary Ion Exchange,« *Journal of the American Ceramic Society*, vol. 62, no. 7-8, pp. 390-395, July 1979.
- [29] R. Oven, D. G. Ashworth and M. C. Page, »On the analysis of field-assisted ion diffusion into glass,« *Journal of Physics: Condensed Matter*, vol. 4, no. 16, p. 4089, 1992.
- [30] S. Batchelor, R. Oven and G. Ashworth, »Characterisation of electric field assisted diffused potassium ion planar optical waveguides,« *Electronics Letters*, vol. 32, no. 22, pp. 2082-2083, 1996.
- [31] N. Godbout and S. Lacroix, »Characterization of thermal poling in silica glasses by current measurements,« *Journal of Non-Crystalline Solids*, vol. 316, no. 2-3, pp. 338-348, 2003.
- [32] A. A. Lipovskii, A. V. Omelchenko and M. I. Petrov, »Modeling charge transfer dynamics and electric field distribution in glasses during poling and electrostimulated diffusion,« *Technical Physics Letters*, vol. 36, no. 11, pp. 1028-1036, 2010.
- [33] M. I. Petrov, A. V. Omelchenko and A. A. Lipovskii, »Electric field and spatial charge formation in glasses and glassy nanocomposites,« *Journal of Applied Physics*, vol. 109, no. 9, p. 094108, 2011.
- [34] R. Oven, »Calculation of the space charge distribution in poled soda-lime glass,« *Journal of Physics: Condensed Matter*, vol. 34, no. 5, p. 055702, 2021.
- [35] R. Oven, »Analytical model of electric field assisted ion diffusion into glass containing two indigenous mobile species, with application to poling,« *Journal of Non-Crystalline Solids*, vol. 553, p. 120476, 2021.
- [36] M. I. Petrov, Y. A. Lepen'kin and A. A. Lipovskii, »Polarization of glass containing fast and slow ions,« *Journal of Applied Physics*, vol. 112, no. 4, p. 043101, 2012.
- [37] A. Einstein, »Über die von der molekularkinetischen Theorie der Wärme geforderte Bewegung von in ruhenden Flüssigkeiten suspendierten Teilchen,« *Annalen der Physik*, vol. 17, pp. 549-560, 1905.
- [38] N. F. Mott and R. W. Gurney, *Electronic processes in ionic crystals*. Clarendon Press, 1948.
- [39] A. B. Lidiard, *Handbuch der Physik*, vol. 20, Berlin: Springer-Verlag, 1957.
- [40] G. K. Batchelor, »Brownian diffusion of particles with hydrodynamic interaction,« *Journal of Fluid Mechanics*, vol. 74, no. 1, pp. 1-29, 9 March 1976.

- [41] J. V. Fitzgerald, »Transference Numbers for Electrical Conduction in Glass,« *The Journal of Chemical Physics*, vol. 20, no. 5, pp. 922-922, 1952.
- [42] A. D. LeClaire, *Physical Chemistry, Solid State*, vol. X, New York: Academic Press, 1970.
- [43] »https://assets.thermofisher.com/TFS-Assets/APD/brochures/objekttraeger_uk_0715_0209.pdf
- [44] A. L. R. Brennand, P. G. Kuansky and J. S. Wilkinson, »Evaluation of Alkali-rich Glasses for Poling,« u *Summaries of Papers Presented at the Lasers and Electro-Optics. CLEO'02. Technical Diges. IEEE*, 2002.
- [45] T. Selvam, P. Pervan, J. Sancho-Parramon, M. C. Spadaro, J. Arbiol and V. Janicki, »Glass poling as a substrate surface pre-treatment for in situ metal nanoparticle formation by reduction of metal salt,« *Surfaces and Interfaces*, vol. 33, p. 102158, 2022.
- [46] https://www.corning.com/media/worldwide/csm/documents/HPFS_Product_Brochure_All_Grades_2015_07_21.pdf
- [47] <https://m.crystran.co.uk/optical-materials/quartz-crystal-sio2>
- [48] <https://www.schott.com/shop/medias/SCHOTT-datasheet-N-KF9.pdf?context=bWFzdGVyfHJvb3R8NDM2MDI4fGFwcGxpY2F0aW9uL3BkZnxoYjMvaGVlZg4Mjl1NjEzNzQyMzgucGRmfGNhNTI4MDc0YTY2NWNhNzI4MDAyNDQxN2JkMWZiMjNlZTI3MWEyYThjNzI3Mzc0TFiODM5MmWU4MWM4YzY3MGY>
- [49] <https://www.schott.com/shop/medias/schott-datasheet-n-bk7-eng.pdf?context=bWFzdGVyfHJvb3R8NDM2MDI4fGFwcGxpY2F0aW9uL3BkZnxoZTUvaDM4Lzg4MTAzMTYxMDM3MTAucGRmfGJjNmI4ZjFmY2Q1NjMxMTE0MjkzMTUwOGRmMTUzOTg2NWJjZTgzMjA0OTc2NTNiMThjN2RhMjI4NGZmMWM4MmWU>
- [50] M. Dussauze, T. Cremoux, F. Adamietz and V. Rodriguez, »Thermal Poling of Optical Glasses: Mechanisms and Second-Order Optical Properties,« *International Journal of Applied Glass Science*, vol. 3, no. 4, pp. 309-320, 2012.